# “Impacts of Fluorescent Base Analogue Substitution on the Folding of a Riboswitch”

Janson E. Hoeher[#], Michael A. Veirs[#], Julia R. Widom[#]*
[#]Department of Chemistry and Biochemistry, University of Oregon
*To whom correspondence should be addressed: jwidom@uoregon.edu

Running title: “Fluorescent Label Alters Riboswitch Folding”

Keywords: 2-aminopurine, circular dichroism, fluorophore, riboswitch, preQ$_1$

Abstract

Riboswitches are gene-regulating mRNA segments most commonly found in bacteria. A riboswitch contains an aptamer domain that binds to a ligand, causing a conformational change in a downstream expression platform. The aptamer domain of the Class I $preQ_1$ riboswitch from *Bacillus subtilis*, which consists of a stem-loop structure and an adenine-rich single-stranded tail (L3), re-folds into a pseudoknot structure upon binding of its ligand, $preQ_1$. To study the role of L3 in ligand recognition, we inserted 2-aminopurine (2-AP), a fluorescent base analogue of adenine (A), into the riboswitch at six different positions within L3. 2-AP differs from A in the relocation of its amino group from C6 to C2, allowing us to directly probe the significance of this specific functional group. We used circular dichroism spectroscopy and thermal denaturation experiments to study the structure and stability, respectively, of the riboswitch in the absence and presence of $preQ_1$. At all labeling positions tested, 2-AP substitution inhibited the ability of $preQ_1$ to stabilize the pseudoknot structure, with its location impacting the severity of the effect. Structural studies of the riboswitch suggest that at the most detrimental labeling sites, 2-AP substitution disrupts non-canonical base pairs. Our results show that these base pairs and tertiary interactions involving other residues in L3 play a critical role in ligand recognition by the $preQ_1$ riboswitch, even at positions that are distal to the ligand binding pocket. They also highlight the importance of accounting for perturbations that fluorescent analogues like 2-AP may exert on the system being studied.

## Introduction

Bacteria employ numerous mechanisms to regulate gene expression in response to physiological cues. A particular niche within this network is filled by riboswitches, which are structured non-coding RNA elements typically found in the 5' untranslated regions of mRNAs (Sherwood and Henkin 2016). A typical riboswitch contains an aptamer domain, which binds to a ligand, and an expression platform, which re-folds in response to ligand binding by the aptamer to regulate expression downstream genes. Riboswitches typically control the transcription or translation step of gene expression, although other mechanisms have also been observed (Caron et al. 2012; Li and Breaker 2013; Rieder et al. 2010). Since their discovery, riboswitches have been the subjects of intensive study due to their utility as molecular sensors (Harbaugh et al. 2017; You et al. 2015) and antibiotic targets (Jia et al. 2013; Blount and Breaker 2006).

The structures and dynamics of riboswitches are intimately linked to their biological functions, as a riboswitch must fold into a native structure capable of ligand binding during the kinetically-controlled process of transcription. As a result, many techniques have been used to probe riboswitch structure and dynamics, including x-ray crystallography (Klein et al. 2009), NMR (Kang et al. 2009; Zhang et al. 2011), single-molecule Förster resonance energy transfer (Widom et al. 2018; Suddala et al. 2013) and bulk fluorescence spectroscopy (Rieder et al. 2010; Petrone et al. 2011). For studies utilizing bulk fluorescence spectroscopy, a common approach is to replace a base within the riboswitch with a fluorescent base analogue (FBA), with the most commonly used FBA being the adenine analogue 2-aminopurine (2-AP; Fig. 1) (Ward and Reich 1969). Ideally, an FBA would not change the structure or function of the RNA while having photophysical properties that are sensitive to its local environment within the RNA. 2-AP satisfies the latter requirement: when it is substituted into RNA or DNA, its fluorescence is quenched in a sequence- and structure-dependent manner, enabling it to be used to monitor the extent of base stacking at specific sites (Jones and Neely 2015). The photophysics of 2-AP have been extensively characterized, revealing that quenching is mediated by static and dynamic mechanisms as well as electron transfer in different structural and sequence contexts (Paterson et al. 2020; Jean and Hall 2001; Liang and Matsika 2011). However, it is not well

known how FBAs such as 2-AP perturb the structure and dynamics of RNA, despite their use in many studies (Gu et al. 2016; Zhao and Xia 2009; Bradrick and Marino 2004; Rist and Marino 2001; Hall and Williams 2004; Ballin et al. 2007). While FBAs are designed to preserve the Watson-Crick base pairing properties of their corresponding native bases (Fig. 1A-B), they may significantly impact structural features of the RNA that rely on non-Watson-Crick interactions. Such interactions are common in the complex 3-dimensional structures that riboswitches and other RNAs can adopt (Butcher and Pyle 2011; Olson et al. 2019). 2-AP differs from A in the relocation of its amino group from C6 to C2, so studies of 2-AP-labeled RNA can be used to infer the significance of this functional group, regardless of whether its fluorescence properties are exploited.

In this study, we investigated the effects of 2-AP substitution on ligand recognition by the preQ$_1$ riboswitch from *Bacillus subtilis*, which is responsible for regulating genes involved in synthesis of the hypermodified nucleobase queuosine (Roth et al. 2007). This riboswitch binds to the metabolic intermediate preQ$_1$, which induces a conformational change that suppresses expression of genes involved in the production of queuosine by enhancing transcription termination (Widom et al. 2018). Its aptamer domain contains a stem-loop structure (P1) followed by an A-rich tail (L3), and preQ$_1$ binding stabilizes a pseudoknot-structured “docked” conformation containing a second helix, P2 (Fig. 1C) (Klein et al. 2009). To investigate the effects of 2-AP on riboswitch folding, we replaced adenine with 2-AP at each of the six consecutive A residues in the L3 domain. Rather than using 2-AP as a site-specific fluorescent probe, as is normally done, we performed absorbance-based measurements that allowed us to directly compare the native riboswitch to variants modified with 2-AP at different positions. Specifically, we used circular dichroism (CD) spectroscopy and thermal denaturation experiments to study the effects of preQ$_1$ on the structure and thermodynamic stability of the riboswitch, respectively. We found that at every labeling site tested, 2-AP impaired the ability of the riboswitch to re-fold in response to preQ$_1$ binding, and also impaired the ability of preQ$_1$ to stabilize the folded pseudoknot structure of the riboswitch. Placing 2-AP distal to the ligand binding pocket destabilized the riboswitch in the absence of preQ$_1$, whereas labeling sites near the ligand binding pocket were most detrimental to ligand recognition. Rather than assuming that FBA substitution is structurally neutral, as is often done, this work uses 2-AP to intentionally introduce site-specific disruptions in the structure. Through this approach, our results reveal that specific tertiary interactions involving the adenine residues in L3 are critical for ligand recognition by the preQ$_1$ riboswitch. Similar interaction patterns likely exist in the numerous riboswitches and other RNAs that adopt pseudoknot architecture(Theimer et al. 2005; Uroda et al. 2019; Huang et al. 2011; Peselis and Serganov 2014).

## Results

The preQ$_1$ riboswitch contains six consecutive A residues in the L3 domain, making it a natural system in which to study the effects of 2-AP substitution on RNA folding. We prepared multiple riboswitch variants, including an unmodified riboswitch that lacked 2-AP and modified variants that contained 2-AP in position 27, 28, 29, 30, 31, or 32 (Fig. 1C). We then recorded CD spectra and melting curves for each variant in the absence and presence of preQ$_1$. While it can be challenging to extract quantitative structural information from the CD spectra of structured RNAs, it allowed us to determine whether different variants adopted similar global structures to one another, and whether their structures changed upon addition of preQ$_1$. Melting curves, which were recorded by monitoring CD and absorbance at a constant wavelength during heating, were used to assess the thermodynamic stability of the riboswitch. Unfolding is typically indicated by an increase in the absorbance signal and a decrease in the CD signal.

We found that in the absence of preQ$_1$, the unmodified riboswitch exhibits a CD spectrum that is similar to those reported for other RNAs that adopt a pseudoknot structure

(Johnson, Kenneth H 1992). When preQ$_1$ was added, the CD spectrum exhibited a pronounced shift to more negative values (Fig. 2A-B), reflecting the shifting of equilibrium from the "pre-docked" (P2 not intact) to the docked (P2 intact) conformation (Widom et al. 2018; Suddala et al. 2013). In the absence of preQ$_1$, the spectra of the modified variants are quite similar to one another and slightly less intense than the spectrum of the unmodified riboswitch (Fig. 2A). This difference indicates that 2-AP substitution causes a change in the electronic coupling between adjacent bases that gives rise to the CD signal (Burin et al. 2009; Ji et al. 2019). A decrease in the CD intensity upon 2-AP substitution is expected because of the differences in the absorption spectra of adenine and 2-AP. However, changes in electronic coupling between adjacent bases could also be caused by a change in structure, as seen when preQ$_1$ was added to the unmodified riboswitch. A change in structure upon 2-AP substitution would indicate that the 6-amino group of the adenine at that position plays an important role in determining the native fold of the riboswitch, leading us to seek further insight into the matter.

Upon addition of preQ$_1$, the spectra of the variants become more distinct, with most exhibiting a general negative shift (Fig. 2B). Of the six 2-AP-modified variants, addition of preQ$_1$ has a substantial effect (causing a change in CD at least half as large as in the unmodified riboswitch) on those with 2-AP at positions 27, 29 and 30; it has a greatly reduced effect (less than half as large as in the unmodified riboswitch) on those with 2-AP at positions 28, 31 and 32 (Fig. 2C-D). At the two extremes, placing 2-AP at position 31 essentially eliminates the riboswitch's response to preQ$_1$, while placing 2-AP at position 29 nearly maintains the behavior of the unmodified riboswitch. The differences in response likely originate from two factors – proximity to the ligand-binding pocket, and tertiary interactions between L3 and P1. A31 and A32 sit immediately adjacent to the ligand-binding pocket, so it is logical that placing 2-AP at those locations would have a substantial effect on the riboswitch's ability to bind to preQ$_1$. NMR and x-ray crystallography structures indicate that A31 normally forms a Hoogsteen base pair with U8, which in turn makes a hydrogen bond with preQ$_1$ (Klein et al. 2009; Kang et al. 2009; Zhang et al. 2011). 2-AP-substitution removes one of the two hydrogen bonds in this Hoogsteen base pair, presumably allowing U8 to move out of position and preventing it from hydrogen-bonding to the ligand (Fig. 3B). Substitution at A32 is nearly as detrimental as at A31, with relocation of its 6-amino group breaking a hydrogen bond between A32 and preQ$_1$ (Fig. 3C). In the crystal structure, A32 additionally makes a Hoogsteen base pair with U9 (Klein et al. 2009), but this interaction is not observed in the NMR structure which, like our data, was recorded in the absence of calcium (Zhang et al. 2011).

Among the labeling sites that are not adjacent to the ligand-binding pocket (positions 27-30), placing 2-AP at position 28 is particularly detrimental to ligand recognition. Of the residues within L3, only A28 makes hydrogen bonds with members of two different base pairs in P1: A5-U22 and G6-C21 (Klein et al. 2009; Kang et al. 2009; Zhang et al. 2011). Replacing A28 with 2-AP would break two of the four hydrogen bonds that bridge these base pairs. In contrast, replacing A27, A29 or A30 with 2-AP breaks hydrogen bonds with only a single base pair in P1. In summary, our CD measurements indicate that 2-AP interferes with the ability of preQ$_1$ to shift the riboswitch's conformational equilibrium toward the docked conformation, with substitution at position 31 being the most detrimental, followed by position 32, 28, 30, 27, and finally 29, at which 2-AP induces minimal perturbations.

To assess the effects of 2-AP substitution on the thermodynamic stability of the riboswitch structure, thermal denaturation measurements were performed by monitoring CD and absorbance signals at 258 nm as the sample was heated. The riboswitch appears to undergo two unfolding transitions (Fig. 4A), one at ~10-25°C and the other at ~50-60°C. We attribute the lower-temperature transition to disruption of tertiary interactions between L3 and P1 ("transition 1"), and the higher-temperature transition to unfolding of the P1 helix ("transition 2"). This assignment is supported by the fact that placing 2-AP in L3 decreases the $T_M$ of transition 1,

while a mutation that disrupts the P2 helix, G12U, does not do so (Fig. 4C). In the absence of preQ$_1$, the melting curves of all variants appear qualitatively similar to each other, but differences emerge when the curves are quantified (Fig. 5). Transition 1 occurs at $T_m$ = 24 ± 2°C in the unmodified riboswitch (Fig. 5C) and at a lower temperature in the 2-AP-modified variants, having a value of $T_m$ = 10.2 ± 0.1°C with 2-AP at position 27. It increases gradually as 2-AP is moved toward the ligand binding pocket to 22.3 ± 0.4°C with 2-AP at position 32, a similar value to that of the unmodified riboswitch. This indicates 2-AP destabilizes L3-P1 interactions most significantly when it is placed near the "hinge" where the two domains adjoin, and less significantly when it is near the ligand-binding pocket. 2-AP has little effect on $T_m$ 2 (Fig. 5E), which is expected because L3 is fully single-stranded at that temperature.

When preQ$_1$ is added to the unmodified riboswitch, transition 1 shifts to a significantly higher temperature, from $T_m$ = 24 ± 2°C to 48 ± 1°C; Fig. 4B and Fig. 5) and narrows (from ΔT = 10.4 ± 0.2°C to 5.6 ± 0.6°C). We thus propose that preQ$_1$ binding stabilizes the L3-P1 interactions that unfold in transition 1. The melting temperature of transition 2 changes only slightly (from 55.4 ± 0.6°C to 59 ± 1.2°C, while its width decreases to a smaller extent than seen for transition 1 (from 4.7 ± 0.1°C to 3.5 ± 0.1°C). As seen with the CD spectra, 2-AP substitution at *any* position dampens the riboswitch's response to preQ$_1$. When 2-AP is placed at position 31 or 32, preQ$_1$ has only a slight effect on the $T_M$ and ΔT of transition 1. The other four modified variants exhibit intermediate behavior, with the variant with 2-AP at position 29 most closely mimicking the unmodified riboswitch, an analogous pattern to what we observed in our CD spectra.

When the CD signal is monitored at 258 nm in the absence of preQ$_1$, all variants exhibit a monotonic decrease in intensity as the temperature is increased, as expected. In the presence of preQ$_1$, all variants except for the one with 2-AP at position 31 exhibit an increase in CD intensity, followed by a decrease starting at ~40 °C (Fig. 6A-B). To investigate this surprising observation, we recorded CD spectra at different temperatures during thermal ramping (Fig. 6C-F). We observed that in the presence of preQ$_1$, the changes in the lineshape of the CD spectrum lead to a transient increase in CD intensity at 258 nm, while the overall intensity of the spectrum decreases monotonically. As a result, we did not attempt to quantitatively interpret our CD melting curves. Instead, we take a transient increase in the melting curve to be an indication that a variant's spectrum undergoes a change in lineshape that is similar to that of the unmodified riboswitch. We thus conclude that variants with 2-AP at position 27, 28, 29, 30 or 32 unfold via an intermediate similar to that seen for the unmodified riboswitch, while variant with 2-AP at position 31 does not. Together, our data indicate that 2-AP substitution at any position within L3 has the effect of destabilizing the riboswitch in the absence of preQ$_1$ (particularly at "hinge" positions) and hindering the ability of preQ$_1$ to stabilize the docked pseudoknot conformation (particularly at positions adjacent to the ligand binding pocket).

## Discussion

The work presented here comprises a systematic study of the effects of 2-AP substitution on the folding of the preQ$_1$ riboswitch. The stretch of six consecutive A residues in the L3 domain allowed us to place 2-AP into several different structural contexts, from "hinge" residues to noncanonical base pairs. In addition to highlighting problems that can arise when utilizing 2-AP as a fluorescent probe, this work provides a map of interactions involving the 6-amino group of adenine (Fig. 7). 2-AP substitution can be thought of as introducing a subtle "mutation", and the deficiencies it induces can be used to infer the role of that functional group when the native adenine is present. Notably, 2-AP substitution was not completely neutral at any of the six labeling positions we tested. While the effects on ligand recognition were most drastic when 2-AP was placed near the ligand-binding pocket, we did not observe monotonic behavior in which disruption simply became more significant as 2-AP was moved closer to the

ligand binding pocket. In fact, in the absence of $preQ_1$, the stability of the riboswitch was most affected when 2-AP was placed in the hinge region at the 5' end of L3 and the magnitude of the perturbations *decreased* as 2-AP was moved toward the ligand-binding pocket. The effects of 2-AP can be attributed to the breaking of hydrogen bonds when the 6-amino group of adenine is relocated to C2 to generate 2-AP. In the case of positions 27-30, these interactions occur between residues in L3 and P1, whereas at positions 31 and 32, hydrogen bonds with the ligand itself or with residues that hydrogen bond to the ligand are impacted. Placing 2-AP at position 28 is more detrimental than would be expected based on its distance from the ligand-binding pocket. This may be because the 6-amino group of A28 makes hydrogen bonds that bridge two different base-pairs in P1 (A5-U22 and G6-C21) (Klein et al. 2009; Kang et al. 2009), making it a more important "linchpin" than the 6-amino groups on other residues in L3.

In addition to yielding insights into the ligand recognition mechanism of the $preQ_1$ riboswitch, this work reveals the challenges that can arise in interpreting measurements that require chemical modification of the system being studied. There has been an increasing appreciation that the fluorescent tags often used in studies of the structure and dynamics of nucleic acids can perturb the very molecules they are being used to study. For example, Jahnke et al. compared the performance of a DNA pH sensor when both it and a "regulator" strand that binds to it were end-labeled with various fluorophores. The affinity of the nanostructure for the regulator strand differed by many orders of magnitude across the different fluorophore combinations (Jahnke et al. 2021). It has also been known for some time that the popular cyanine dyes such as Cy3 are able to stack on the ends of double-stranded nucleic acids, stabilizing the duplexes in the process (Moreira et al. 2015). It is not immediately obvious what effects substitution of fluorescent base analogues such as 2-AP should have on the nucleic acids of interest - quite intentionally, they bear far more chemical similarity to components that occur naturally in nucleic acids than do larger artificial dyes. In particular, they are typically designed to maintain Watson-Crick base pairing, and some examples exist that also maintain Hoogsteen base pairing (Rovira et al. 2015; Hawkins et al. 2001). However, as FBAs are substituted in for native bases rather than tethered flexibly to the RNA, any perturbations to hydrogen bonding or base stacking could have significant consequences. Further insight into the key interactions that drive RNA folding could be obtained by investigating a panel of variants with different FBAs at the site of interest, as each FBA would induce a slightly different perturbation of geometry and/or hydrogen bonding.

In summary, we observed that 2-AP substitution at different positions exerts significant and varied perturbations on riboswitch behavior. We identified key interactions, such as the Hoogsteen base-pair between A31 and U8 and tertiary interactions between A28 and P1, that are critical for ligand recognition, observations that are supported by the high level of sequence conservation in L3 (Roth et al. 2007). Other riboswitches that adopt pseudoknot structures, particularly ones that contain A-rich domains like L3 (Panchapakesan et al. 2021), are likely to take advantage of similar interactions.

## Methods and Materials

RNA oligonucleotides were purchased from Dharmacon and DNA oligonucleotides were purchased from Integrated DNA Technologies (sequences in table 1). All RNA oligonucleotides were HPLC-purified by the manufacturer, and 3' segments were purchased with a 5' phosphate to enable ligation. Riboswitch samples were prepared by splinted ligation using T4 RNA ligase 2 (New England Biolabs M0239S). 5 nanomoles each of the 5' and 3' segments of the riboswitch and the DNA splint were combined and heated to 90 °C for 2 minutes and then allowed to cool to RT over 10 minutes. The manufacturer-provided RNA ligase 2 reaction buffer was added 30 seconds into cooling. After cooling, the mixture was diluted in reaction buffer to a total volume of 150 µL and 60 units of T4 RNA ligase 2 were added. The reactions were incubated at room

temperature for 3 hours, then resolved on a 15% polyacrylamide-urea gel. The product band was recovered from the gel by electroelution using a BioRad model 422 electro-eluter followed by ethanol precipitation.

All CD spectra and melting curves were recorded on a Jasco J-1500 spectrometer in a buffer consisting of 20 mM $Na_iPO_4$ at pH 7.5 and 100 mM NaCl. The samples were heated to 90 °C for 2 minutes and then crash cooled in ice water for 10 minutes before measurement in order to allow the RNA to fold without dimerizing. The CD spectra were recorded in a 1 cm path-length cuvette (Starna 16.160-10) with the riboswitch at a concentration of 2 µM. Scans were performed from 350 nm to 195 nm at a rate of 10 nm per minute with an integration time of 4 seconds and an excitation bandwidth of 2 nm. The spectra presented here are the average of 4 sequential scans. Melting curves were recorded during heating from 4 °C to 80 °C at a rate of 0.75 °C per minute while monitoring CD and absorbance at a wavelength of 258 nm. A 1 cm path-length, low head-space cuvette (Starna 26.160/LHS) was used for these measurements. Before every use, the cuvettes were soaked in a 1% Hellmanex solution at 35 °C for 30 minutes and then rinsed with MilliQ water and dried with nitrogen gas. Spectra were background-corrected by subtracting off a buffer scan (including $preQ_1$ where appropriate) and then converted from units of millidegrees to extinction coefficient (L/mol*cm) using the following equation, where *CD* is the signal in millidegrees, *C* is the concentration in mol/L and *L* is the path length in cm:

$$\Delta\varepsilon = \frac{CD}{32980 \cdot C \cdot L}$$

Finally, they were converted to Δε per nucleotide by dividing by the number of nucleotides in the riboswitch, 38.

A fitting procedure was performed in Mathematica (Wolfram Research) to extract melting temperatures ($T_m$) and transition widths ($\Delta T$) from melting curves (Mergny and Lacroix 2003). First, a linear fit was performed on the segment of the melting curve recorded between 75 and 80 °C, which was extrapolated to lower temperature. The absorbance vs. temperature curve was then converted to a proxy for the “fraction folded” at temperature *T*, θ(*T*), using the following equation:

$$\theta(T) = \frac{L(T) - A(T)}{L(T) - A(T_{min})}$$

where $L(T)$ is the value of the linear fit mentioned above at temperature *T*, $A(T)$ is the recorded absorbance at temperature *T*, and $A(T_{min})$ is the recorded absorbance at the lowest temperature. This rescales the signal to run from 1 to 0 and utilizes the linear fit to correct for the temperature dependence of absorbance that occurs in the absence of any specific unfolding transition. $\theta(T)$ was then fit using the following equation:

$$\theta(T) = \frac{a}{1 + e^{(T - T_{M1})/\Delta T1}} + \frac{b}{1 + e^{(T - T_{M2})/\Delta T2}}$$

where *a* and *b* are the weights, $T_{M1}$ and $T_{M2}$ are the melting temperatures, and $\Delta T1$ and $\Delta T2$ are the widths of unfolding transitions 1 and 2, respectively. Each experimental replicate was fit individually, then the average and standard deviation of the resulting parameter values were determined.

References

Ballin JD, Bharill S, Fialcowitz-White EJ, Gryczynski Zi, Gryczynski Z, Wilson GM. 2007. Site-Specific Variations in RNA Folding Thermodynamics Visualized by 2-Aminopurine Fluorescence. *Biochemistry* **46**: 13948–13960.

Blount KF, Breaker RR. 2006. Riboswitches as antibacterial drug targets. *Nat Biotechnol* **24**: 1558–1564.

Bradrick TD, Marino JP. 2004. Ligand-induced changes in 2-aminopurine fluorescence as a probe for small molecule binding to HIV-1 TAR RNA. *RNA* **10**: 1459–1468.

Burin AL, Armbruster ME, Hariharan M, Lewis FD. 2009. Sum rules and determination of exciton coupling using absorption and circular dichroism spectra of biological polymers. *Proc Natl Acad Sci* **106**: 989–994.

Butcher SE, Pyle AM. 2011. The Molecular Interactions That Stabilize RNA Tertiary Structure: RNA Motifs, Patterns, and Networks. *Acc Chem Res* **44**: 1302–1311.

Caron M-P, Bastet L, Lussier A, Simoneau-Roy M, Massé E, Lafontaine DA. 2012. Dual-acting riboswitch control of translation initiation and mRNA decay. *Proc Natl Acad Sci* **109**: E3444–E3453.

Gu X, Park S-Y, Tonelli M, Cornilescu G, Xia T, Zhong D, Schroeder SJ. 2016. NMR Structures and Dynamics in a Prohead RNA Loop that Binds Metal Ions. *J Phys Chem Lett* **7**: 3841–3846.

Hall KB, Williams DJ. 2004. Dynamics of the IRE RNA hairpin loop probed by 2-aminopurine fluorescence and stochastic dynamics simulations. *RNA* **10**: 34–47.

Harbaugh SV, Goodson MS, Dillon K, Zabarnick S, Kelley-Loughnane N. 2017. Riboswitch-Based Reversible Dual Color Sensor. *ACS Synth Biol* **6**: 766–781.

Hawkins ME, Pfleiderer W, Jungmann O, Balis FM. 2001. Synthesis and Fluorescence Characterization of Pteridine Adenosine Nucleoside Analogs for DNA Incorporation. *Anal Biochem* **298**: 231–240.

Huang L, Ishibe-Murakami S, Patel DJ, Serganov A. 2011. Long-range pseudoknot interactions dictate the regulatory response in the tetrahydrofolate riboswitch. *Proc Natl Acad Sci* **108**: 14801–14806.

Jahnke K, Grubmüller H, Igaev M, Göpfrich K. 2021. Choice of fluorophore affects dynamic DNA nanostructures. *Nucleic Acids Res*. https://doi.org/10.1093/nar/gkab201 (Accessed April 5, 2021).

Jean JM, Hall KB. 2001. 2-Aminopurine fluorescence quenching and lifetimes: Role of base stacking. *Proc Natl Acad Sci* **98**: 37–41.

Ji H, Johnson NP, von Hippel PH, Marcus AH. 2019. Local DNA Base Conformations and Ligand Intercalation in DNA Constructs Containing Optical Probes. *Biophys J* **117**: 1101–1115.

Jia X, Zhang J, Sun W, He W, Jiang H, Chen D, Murchie AIH. 2013. Riboswitch Control of Aminoglycoside Antibiotic Resistance. *Cell* **152**: 68–81.

Johnson, Kenneth H G Donald M. 1992. Analysis of an RNA Pseudoknot Structure by CD Spectroscopy. *J Biomol Struct Dyn* **9**: 733–745.

Jones AC, Neely RK. 2015. 2-aminopurine as a fluorescent probe of DNA conformation and the DNA-enzyme interface. *Q Rev Biophys* **48**: 244–279.

Kang M, Peterson R, Feigon J. 2009. Structural Insights into Riboswitch Control of the Biosynthesis of Queuosine, a Modified Nucleotide Found in the Anticodon of tRNA. *Mol Cell* **33**: 784–790.

Klein DJ, Edwards TE, Ferré-D'Amaré AR. 2009. Cocrystal structure of a class I preQ$_1$ riboswitch reveals a pseudoknot recognizing an essential hypermodified nucleobase. *Nat Struct Mol Biol* **16**: 343–344.

Li S, Breaker RR. 2013. Eukaryotic TPP riboswitch regulation of alternative splicing involving long-distance base pairing. *Nucleic Acids Res* **41**: 3022–3031.

Liang J, Matsika S. 2011. Pathways for Fluorescence Quenching in 2-Aminopurine π-Stacked with Pyrimidine Nucleobases. *J Am Chem Soc* **133**: 6799–6808.

Mergny J-L, Lacroix L. 2003. Analysis of Thermal Melting Curves. *Oligonucleotides* **13**: 515–537.

Moreira BG, You Y, Owczarzy R. 2015. Cy3 and Cy5 dyes attached to oligonucleotide terminus stabilize DNA duplexes: Predictive thermodynamic model. *Biophys Chem* **198**: 36–44.

Olson WK, Li S, Kaukonen T, Colasanti AV, Xin Y, Lu X-J. 2019. Effects of Noncanonical Base Pairing on RNA Folding: Structural Context and Spatial Arrangements of G·A Pairs. *Biochemistry* **58**: 2474–2487.

Panchapakesan SSS, Corey L, Malkowski SN, Higgs G, Breaker RR. 2021. A second riboswitch class for the enzyme cofactor NAD+. *RNA* **27**: 99–105.

Paterson KA, Arlt J, Jones AC. 2020. Dynamic and static quenching of 2-aminopurine fluorescence by the natural DNA nucleotides in solution. *Methods Appl Fluoresc* **8**: 025002.

Peselis A, Serganov A. 2014. Structure and function of pseudoknots involved in gene expression control. *WIREs RNA* **5**: 803–822.

Petrone PM, Dewhurst J, Tommasi R, Whitehead L, Pomerantz AK. 2011. Atomic-scale characterization of conformational changes in the preQ1 riboswitch aptamer upon ligand binding. *J Mol Graph Model* **30**: 179–185.

Rieder U, Kreutz C, Micura R. 2010. Folding of a transcriptionally acting PreQ1 riboswitch. *Proc Natl Acad Sci USA* **107**: 10804–10809.

Rist M, Marino JP. 2001. Association of an RNA kissing complex analyzed using 2-aminopurine fluorescence. *Nucleic Acids Res* **29**: 2401–2408.

Roth A, Winkler WC, Regulski EE, Lee BWK, Lim J, Jona I, Barrick JE, Ritwik A, Kim JN, Welz R, et al. 2007. A riboswitch selective for the queuosine precursor preQ1 contains an unusually small aptamer domain. *Nat Struct Mol Biol* **14**: 308–317.

Rovira AR, Fin A, Tor Y. 2015. Chemical Mutagenesis of an Emissive RNA Alphabet. *J Am Chem Soc* **137**: 14602–14605.

Sherwood AV, Henkin TM. 2016. Riboswitch-Mediated Gene Regulation: Novel RNA Architectures Dictate Gene Expression Responses. *Annu Rev Microbiol* **70**: 361–374.

Suddala KC, Rinaldi AJ, Feng J, Mustoe AM, Eichhorn CD, Liberman JA, Wedekind JE, Al-Hashimi HM, Brooks CL III, Walter NG. 2013. Single transcriptional and translational preQ$_1$ riboswitches adopt similar pre-folded ensembles that follow distinct folding pathways into the same ligand-bound structure. *Nucleic Acids Res* **41**: 10462–10475.

Theimer CA, Blois CA, Feigon J. 2005. Structure of the Human Telomerase RNA Pseudoknot Reveals Conserved Tertiary Interactions Essential for Function. *Mol Cell* **17**: 671–682.

Uroda T, Anastasakou E, Rossi A, Teulon J-M, Pellequer J-L, Annibale P, Pessey O, Inga A, Chillón I, Marcia M. 2019. Conserved Pseudoknots in lncRNA MEG3 Are Essential for Stimulation of the p53 Pathway. *Mol Cell* **75**: 982-995.e9.

Ward DC, Reich E. 1969. Fluorescence Studies of Nucleotides and Polynucleotides. *J Biol Chem* **244**: 1228–1237.

Widom JR, Nedialkov YA, Rai V, Hayes RL, Brooks CL III, Artsimovitch I, Walter NG. 2018. Ligand Modulates Cross-Coupling between Riboswitch Folding and Transcriptional Pausing. *Mol Cell* **72**: 541–552.

You M, Litke JL, Jaffrey SR. 2015. Imaging metabolite dynamics in living cells using a Spinach-based riboswitch. *Proc Natl Acad Sci USA* **112**: E2756–E2765.

Zhang Q, Kang M, Peterson RD, Feigon J. 2011. Comparison of Solution and Crystal Structures of PreQ1 Riboswitch Reveals Calcium-Induced Changes in Conformation and Dynamics. *J Am Chem Soc* **133**: 5190–5193.

Zhao L, Xia T. 2009. Probing RNA conformational dynamics and heterogeneity using femtosecond time-resolved fluorescence spectroscopy. *Methods* **49**: 128–135.

| | |
|---|---|
| Unmodified | 5’ GCA GAG GUU CUA GCU ACA \| CCC UCU AUA AAA AAC UAA GG |
| Position 27 | 5’ GCA GAG GUU CUA GCU ACA \| CCC UCU AU**(2-AP)** AAA AAC UAA GG |
| Position 28 | 5’ GCA GAG GUU CUA GCU ACA \| CCC UCU AUA **(2-AP)**AA AAC UAA GG |
| Position 29 | 5’ GCA GAG GUU CUA GCU ACA \| CCC UCU AUA A**(2-AP)**A AAC UAA GG |
| Position 30 | 5’ GCA GAG GUU CUA GCU ACA \| CCC UCU AUA AA**(2-AP)** AAC UAA GG |
| Position 31 | 5’ GCA GAG GUU CUA GCU ACA \| CCC UCU AUA AAA **(2-AP)**AC UAA GG |
| Position 32 | 5’ GCA GAG GUU CUA GCU ACA \| CCC UCU AUA AAA A**(2-AP)**C UAA GG |
| G12U mutant | 5’ GCA GAG GUU CUA **U**CU ACA \| CCC UCU AUA AAA AAC UAA GG |
| DNA splint | 5’ GTT TTT TAT AGA GGG TGT AGC TAG AAC C |

Table 1: Sequences of oligonucleotides used in this work. Bold text highlights the positions of 2-AP substitutions or mutations. Vertical lines indicate the division between the 5’ and 3’ segments that were ligated together. Each 3’ segment was purchased with a phosphate group at its 5’ end to enable ligation.

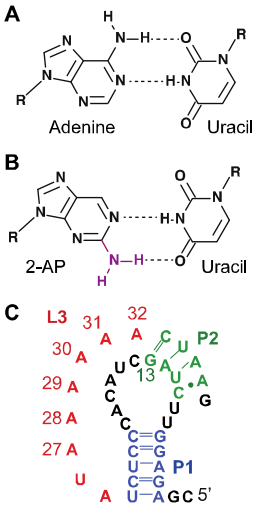


Figure 1: (A) Chemical structure of a Watson-Crick base pair between adenine and uracil. (B) Chemical structure of a Watson-Crick base pair between 2-aminopurine and uracil. The re-positioned amine group is shown in purple. (C) The pre$Q_1$ riboswitch in its docked pseudoknot conformation. The P1, P2 and L3 domains are indicated in blue, green and red, respectively. Numbers indicate the site at which a mutation was investigated (G13) and the six 2-AP labeling sites (A27-A32).

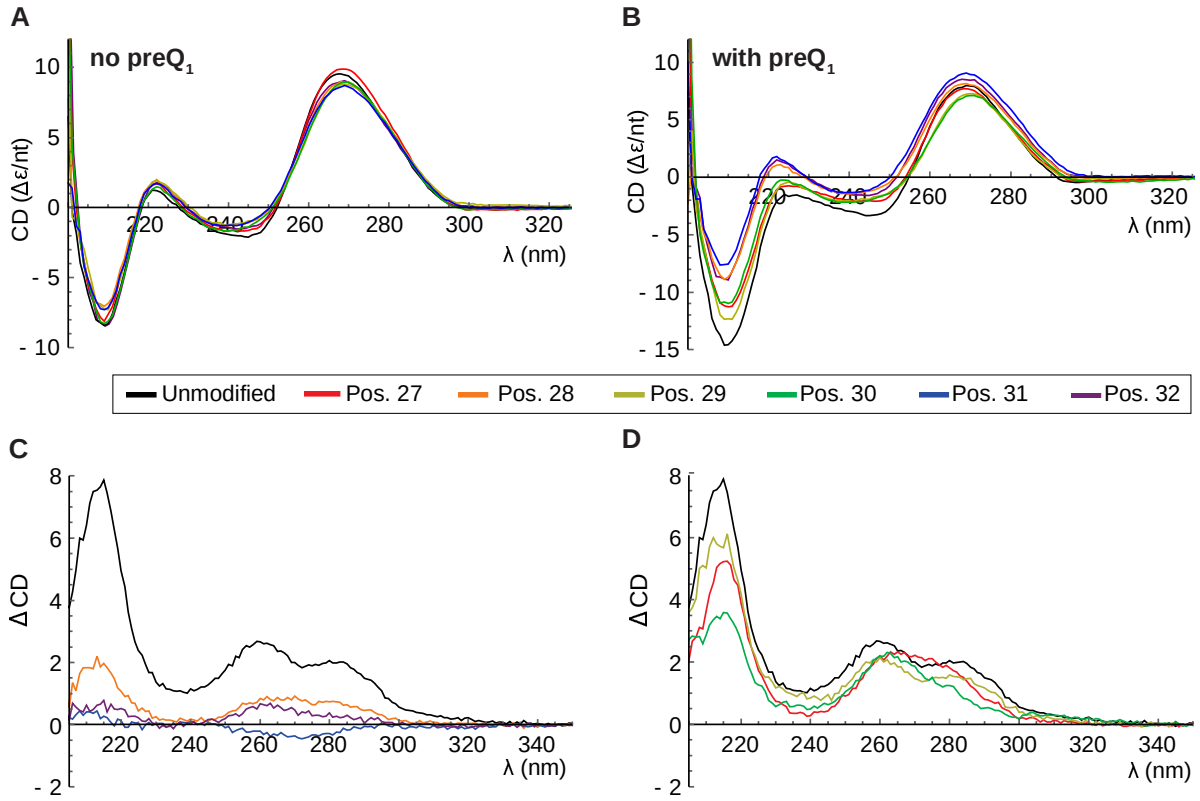


Figure 2: CD spectra of riboswitch variants. (A-B) Overlaid spectra of the unmodified and modified riboswitches in the absence (A) or presence (B) of 5 µM $preQ_1$. (C-D) Difference spectra where the CD spectrum recorded in the presence of ligand has been subtracted from the CD spectrum recorded in the absence of ligand. (C) Difference spectra for unmodified riboswitch and variants with 2-AP at positions 28, 31 and 32, in which the effect of $preQ_1$ is greatly reduced. (D) Difference spectra for unmodified riboswitch and variants with 2-AP at positions 27, 29 and 30, in which the effect of $preQ_1$ remains substantial despite 2-AP substitution.

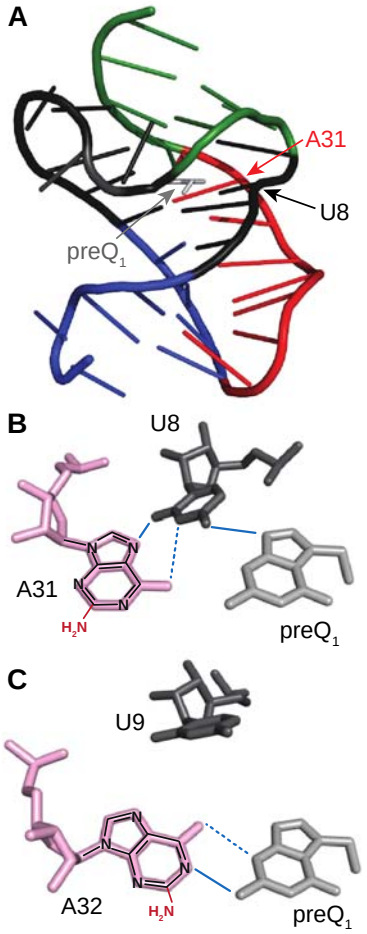


Figure 3: 2-AP disrupts key hydrogen bonds when placed at positions 31 or 32. (A) NMR structure of the riboswitch (PDB ID 2L1V) with the locations of the ligand, U8 and A31 indicated. (B) Closeup of the ligand-binding pocket showing interactions between U8, A31 and $preQ_1$. Hydrogen bonds are indicated by blue lines, with dashed lines indicating bonds that are broken when A is replaced by 2-AP. (C) Closeup of the ligand binding pocket viewed from the same perspective showing interactions between A32 and $preQ_1$.

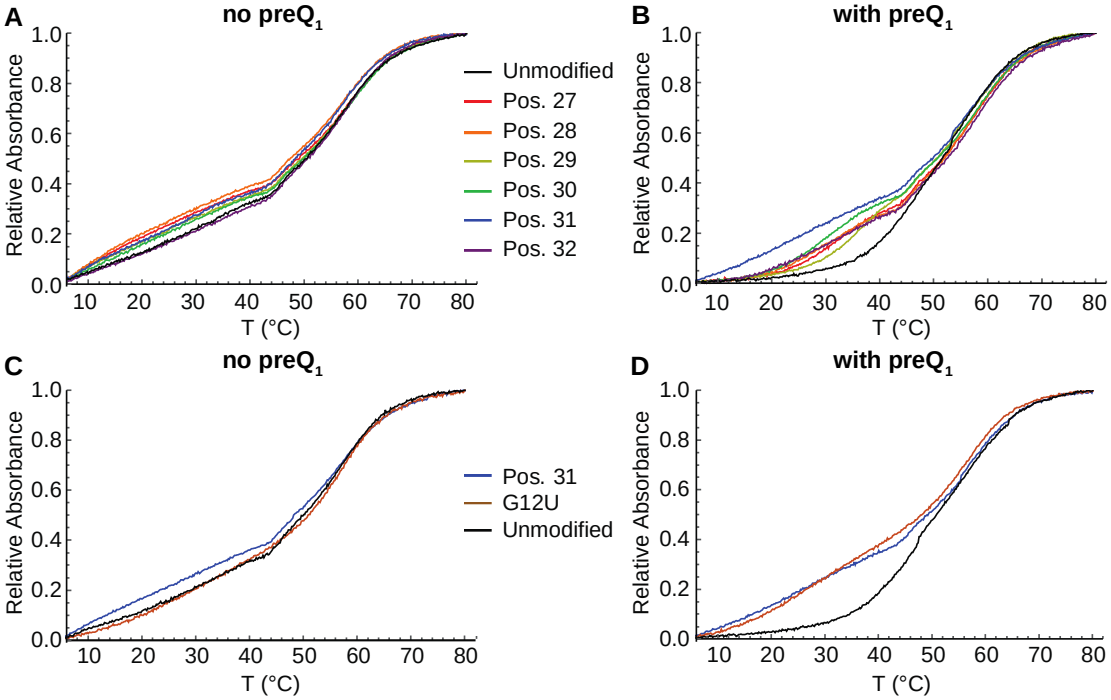


Figure 4: (A-B) Absorbance melting curves of unmodified and 2-AP-modified variants recorded at 258 nm in the absence (A) or presence (B) of 5 µM $preQ_1$. (C-D) Melting curves of unmodified and position 31-modified variants and G12U mutant in the absence (C) or presence (D) of 2 µM $preQ_1$. For ease of comparison, the curves were shifted and then normalized to run from a minimum of 0 to a maximum of 1.

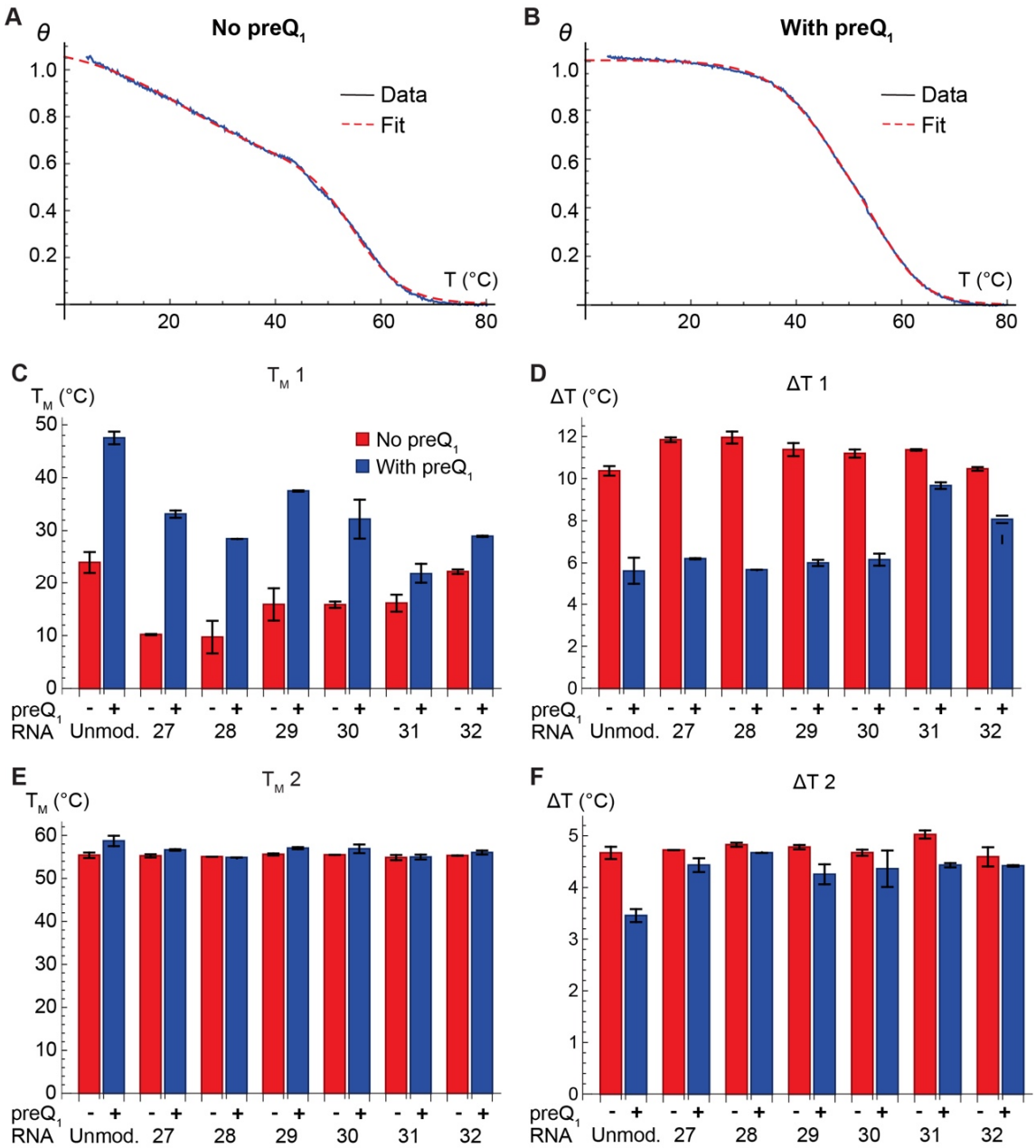


Figure 5: (A-B) Processed melting curves and fits for the unmodified riboswitch plotted as θ (see methods) vs. T in the absence (A) or presence (B) of 5 μM $preQ_1$. (C-F) Fitting parameters extracted from absorbance melting curves. Error bars represent the standard deviation of two replicates. (C) Melting temperature of transition 1 for the unmodified riboswitch ("Unmod.") and all 2-AP-modified variants (27-32) in the absence (red) or presence (blue) of $preQ_1$. (D) Width of transition 1. (E) Melting temperature of transition 2. (F) Width of transition 2.

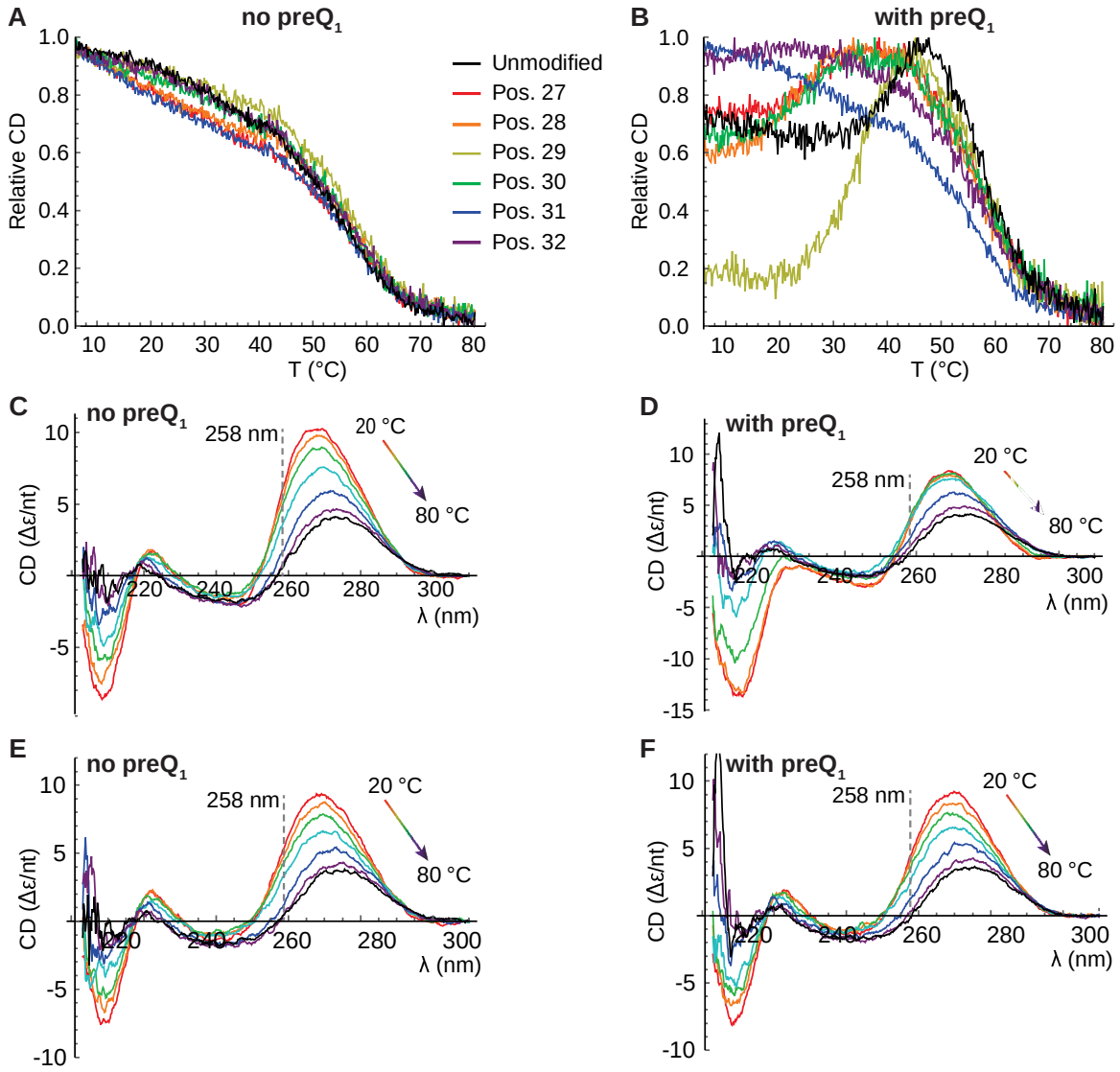


Figure 6: (A-B) CD melting curves of unmodified and 2-AP-modified variants recorded at 258 nm in the absence (A) or presence (B) of 5 µM $preQ_1$. For ease of comparison, the curves were shifted and normalized to run from a minimum of 0 to a maximum of 1. (C-F) CD spectra recorded during thermal ramping at 20 (red), 30 (orange), 40 (green), 50 (cyan), 60 (blue), 70 (purple) and 80 (black) °C. The wavelength at which the CD was monitored while recording melting curves is indicated by a dashed line. (C) Unmodified riboswitch in the absence of $preQ_1$. (D) Unmodified riboswitch in the presence of 5 µM $preQ_1$. (E) Position 31 variant in the absence of $preQ_1$. (F) Position 31 variant in the presence of 5 µM $preQ_1$.

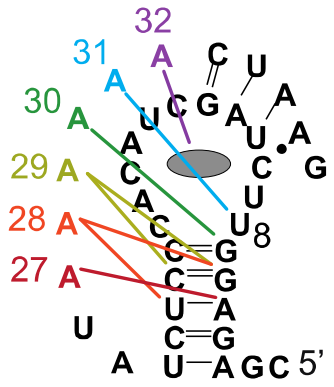


Figure 7: Tertiary interactions involving N6 of adenine residues in L3 based on NMR and crystal structures. Colored lines indicate hydrogen bonds involving N6 of the adenine residue with the same color. $PreQ_1$ is shown as a gray oval.